16 August 2001

PHYSICS LETTERS B

ELSEVIER

Physics Letters B 514 (2001) 233–239

www.elsevier.com/locate/npe

Electric and nuclear transition strength in ^{30,32}Mg

V. Chisté [a,b], A. Gillibert [a], A. Lépine-Szily [b], N. Alamanos [a], F. Auger [a], J. Barrette [c], F. Braga [a], M.D. Cortina-Gil [d], Z. Dlouhy [e], V. Lapoux [a], M. Lewitowicz [d], R. Lichtenthäler [b], R. Liguori Neto [b], S.M. Lukyanov [f,g], M. MacCormick [d], F. Marie [a], W. Mittig [d], F. de Oliveira Santos [d], N.A. Orr [f,g], A.N. Ostrowski [h], S. Ottini [a], A. Pakou [i], Yu.E. Penionzhkevich [f,g], P. Roussel-Chomaz [d], J.L. Sida [a]

[a] *CEA-Saclay, DAPNIA-SPhN, Gif-sur-Yvette, France*
[b] *Instituto de Fisica-Universidade de São Paulo, C.P. 66318, 05389-970 São Paulo, Brazil*
[c] *Department of Physics, McGill University, Montreal, Canada*
[d] *GANIL, Bld Henri Becquerel, BP 5027, 14021 Caen Cedex, France*
[e] *Institute of Nuclear Physics, Academy of Science of Czech Republic, CS 250 68 Rez, Czech Republic*
[f] *Laboratory of Nuclear Reactions, JINR, PO Box 79, Dubna, Russia*
[g] *LPC, IN2P3-CNRS, ISMRA-Université de Caen, 14050 Caen Cedex, France*
[h] *Department of Physics & Astronomy, University of Edinburgh, Edinburgh, EH9 3JZ, UK*
[i] *Department of Physics, The University of Ioannina, 451 10 Ioannina, Greece*

Received 2 March 2001; received in revised form 12 June 2001; accepted 25 June 2001
Editor: V. Metag

Abstract

The charge and mass transition matrix elements of the neutron-rich isotopes ^{30,32}Mg have been extracted from inelastic scattering on ^{208}Pb and ^{12}C targets at 32 *A* MeV. The measured inelastic cross sections for the first 2^+ states were compared to coupled-channels calculations, which take into account the feeding from higher excited states. The method was tested with ^{24}Mg inelastic scattering data obtained in the same experiment. In the framework of the rotational model, the charge and mass deformations are identical and large ($|\beta| \sim 0.5$–0.6) for both isotopes. © 2001 Elsevier Science B.V. All rights reserved.

PACS: 21.10.Dr; 21.10.-k; 25.70.Hi; 27.20+t

The behaviour of magic numbers for nuclei far from stability has been an issue of much interest in nuclear structure ever since the neutron rich Na and Mg nuclei around $N = 20$ were found to be more bound than predicted by a spherical closed-shell prescription [1]. Shell model calculations [2–6] have demonstrated that for $Z = 10$–12 and $N = 19$–22, the $2\hbar\omega$ configurations arising from the excitation of a pair of neutrons across the $N = 20$ shell gap to the fp-orbitals are more strongly bound than the $0\hbar\omega$ states and dominate ground-state configurations, producing the so-called “island of inversion” [3]. A related question is whether in these extreme conditions the deformation of proton and neutron distributions is identical or if a decoupling of the densities occurs. Identical deformations are predicted in the relativistic mean field [7] and in the antisymmetrized molecular model [8], whereas different deformations are obtained in the

E-mail address: agillibert@cea.fr (A. Gillibert).

PII: S0370-2693(01)00796-1

Hartree–Fock–Bogoliubov (HFB) [9] and in the standard shell model [6]. Recent constrained HF calculations with a separable monopole interaction [10] predict similar proton and neutron deformations.

An experimental determination of the neutron and proton deformations of ^{24,30,32}Mg was undertaken at GANIL (Caen, France) via inelastic scattering of secondary ^{24,30,32}Mg beams on ^{208}Pb and ^{12}C targets. For the $N = Z$ ^{24}Mg nucleus, the deformation parameters are well known [11] and were used to test our method, whereas for ^{30,32}Mg only Coulomb excitation was measured previously [12,13]. A primary beam of 77 A MeV ^{36}S was used to produce secondary ^{24,30,32}Mg beams of 37 A MeV with the LISE spectrometer [14] and an achromatic Be degrader. The intensities of ^{24,30,32}Mg secondary beams were, respectively, 2800/s, 1800/s and 36/s, while the corresponding purities were 98%, 88% and 10%. The beam profiles were measured using a pair of drift chambers located in front of and behind the target (cd1 and cd2 in Fig. 1). Reaction targets of 200 mg/cm^2 of ^{208}Pb and 80 mg/cm^2 of ^{12}C were used. The beam energy was 32 A MeV at the target mid-point for both targets. The experimental set-up is shown in Fig. 1. The charged particle detection system consisted of three Si telescopes. The telescope Si$_3$ was used to stop the secondary beam and to detect scattered particles at very forward angles (0–2.1° with respect to the beam axis). Two annular telescopes (Si$_2$, Si$_1$) were employed to detect the scattered Mg nuclei over angular ranges of 2.1°–4.5° and 4.5°–10.0°, respectively. The angular range in the present experiment was larger than in earlier experiments [12,13], covering the domain of both Coulomb and nuclear excitations.

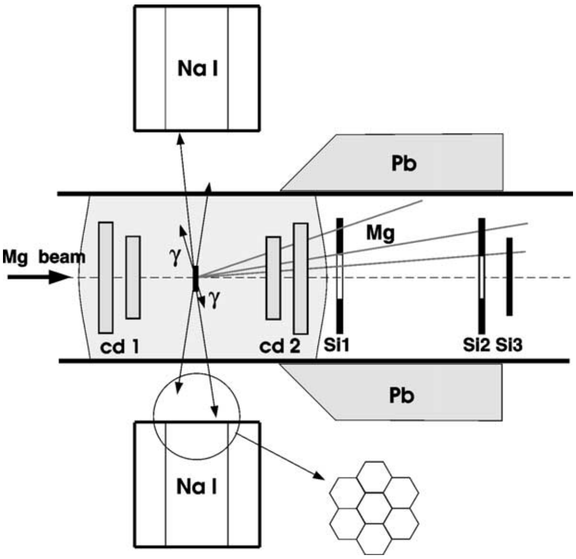

Fig. 1. Experimental set-up.

The secondary beams could be clearly identified event-by-event in ΔE–TOF and ΔE–E spectra. The time-of-flight (TOF) was measured before the reaction target between a micro-channel plate (MCP) detector placed at the second image point of the LISE spectrometer and the cyclotron radio-frequency signal. Due to the selection with the achromatic degrader and Lise, the resolution of the time of flight was enough to separate ^{32}Mg from the main impurities ^{32,33}Al and ^{34,35}Si. The inelastic events were not separated from elastic events in the ΔE–E locii due to the large momentum spread of the beam. The inelastically scattered events were instead identified by the γ-ray deexcitation measured in coincidence with the Mg nuclei. For the detection of the γ rays, we used two sets of 7 hexagonal NaI (length = 20 cm and diameter = 15.8 cm) at $\sim 90°$ relative to the beam axis; 7 above and 7 below the target, 17 cm from the target. The absolute photo-peak efficiencies ($\sim 5.5 \times 10^{-3}$) and energy resolution ($\sim 7\%$) were determined for γ-rays of 0.6616 MeV from a ^{137}Cs source and 1.173 and 1.333 MeV from ^{60}Co decay, using sources of known activity mounted on the target holder. The efficiency for other γ-ray energies was interpolated by a simulation based on the GEANT code. A layer of lead was used to shield the γ detectors from γ-rays produced in reactions of Mg nuclei with the Si detectors. The Doppler-shift and broadening due to the in-flight γ-ray emission of the scattered Mg nuclei was corrected on a event-by-event basis using the relative angle between the scattered Mg nuclei (measured in the drift chamber behind the target) and the NaI detector registering the coincident γ-ray.

In Fig 2. we display the Doppler corrected energy spectra of the γ-rays measured in the NaI array in coincidence with the Mg particles detected in the Si telescopes for the ^{24}Mg + ^{12}C, ^{30}Mg + ^{12}C and ^{32}Mg + ^{12}C reactions (most of the inelastic scattering cross-section is concentrated in Si$_3$ due to the inverse kinematics). A peak at 0.885 MeV, clearly seen in the ^{32}Mg spectrum, corresponds to the transition from the

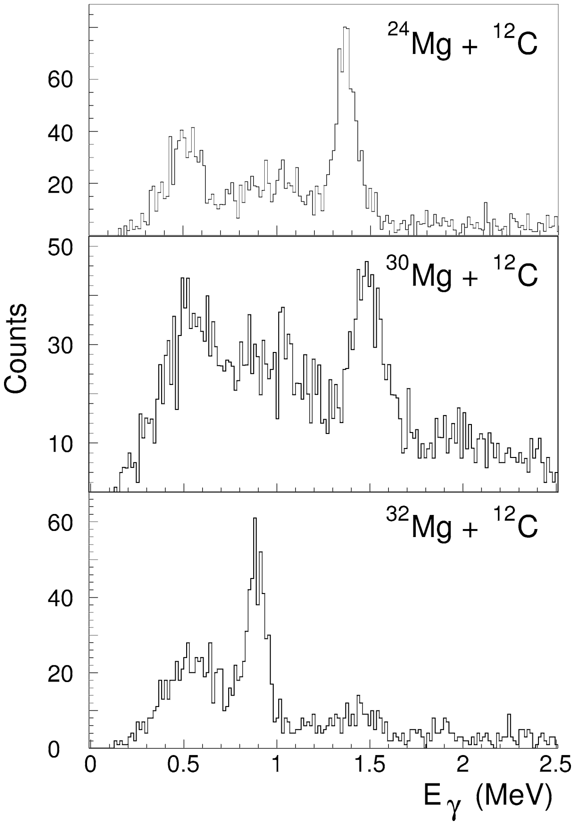

Fig. 2. Doppler corrected γ-ray spectra for the $^{24}Mg + ^{12}C$, $^{30}Mg + ^{12}C$ and $^{32}Mg + ^{12}C$ reactions.

first 2^+ state to the ground-state [15] and a smaller peak at ~ 1.44 MeV is associated with the decay from a state at 2.321 MeV [16] to the 0.885 MeV state. In the ^{30}Mg spectrum, the 1.482 MeV transition from the first 2^+ state to the ground-state [17] is observed. The anisotropy of the γ-rays was estimated for both pure Coulomb or nuclear excitations and pure E2 transitions. Its contribution, though small, was included in the final uncertainty.

The experimental de-excitation cross-section, σ_{exp}, integrated in angle, is defined as

$$\sigma_{\mathrm{exp}} = \frac{N_{\mathrm{coin}}}{N_{\mathrm{inc}} N_{\mathrm{target}} \epsilon(\mathrm{NaI}) \epsilon(\mathrm{Si})} = \frac{S_{\mathrm{exp}}}{\epsilon(\mathrm{Si})} = \frac{S_{\mathrm{exp}}(\mathrm{Si}_k)}{\epsilon(\mathrm{Si}_k)}, \tag{1}$$

where, the number of coincidences N_{coin} was determined after subtracting the underlying background and the contribution from accidental coincidences, N_{inc} is the total number of incident projectiles, N_{target} the number of target atoms per cm^2, ϵ(NaI) the photopeak efficiency of the NaI detectors and $\epsilon(\mathrm{Si}_k)$ the probability for detecting an inelastic event in the kth Si telescope ($k = 1, 2, 3$).

The detection probabilities $\epsilon(\mathrm{Si}_k)$ ($k = 1, 2, 3$) were calculated using a Monte Carlo simulation where the measured profile of the incident secondary beam, the angular straggling in the target, and the geometry of the respective Si_k telescope were included. It took into account the scattering probability $f(\theta)$ as a function of the laboratory angle θ (obtained from the calculated inelastic angular distribution),

$$f(\theta) = \frac{d\sigma}{d\Omega}(\theta)\, d\Omega \Big/ \int_0^{4\pi} \frac{d\sigma}{d\Omega}(\theta)\, d\Omega.$$

The detection probability for the ^{208}Pb target was largest for Si_1 (~ 0.55) decreasing to ~ 0.20 for Si_2, and being almost negligible for Si_3. The experimental quantity $S_{\mathrm{exp}}(\mathrm{Si}_k)$, which represents the fraction of the de-excitation cross-section measured in the respective kth Si telescope, is presented in Table 1 together with the angle-integrated experimental de-excitation cross-sections $\sigma_{\mathrm{exp}}(\mathrm{Si}_k) = S_{\mathrm{exp}}(\mathrm{Si}_k)/\epsilon(\mathrm{Si}_k)$. The ratios $S_{\mathrm{exp}}(\mathrm{Si}_k)/\epsilon(\mathrm{Si}_k)$ are fairly constant, within the experimental uncertainties, proving the correctness of our detection probabilities $\epsilon(\mathrm{Si}_k)$. The adopted value of the angle-integrated experimental de-excitation cross-section $\sigma_{\mathrm{exp}}(2^+ \to 0^+)$ was calculated by dividing the sum of $S_{\mathrm{exp}}(\mathrm{Si}_k)$ by the sum of $\epsilon(\mathrm{Si}_k)$.

In Fig. 3 we present the inelastic scattering angular distributions for the $^{24}Mg + ^{208}Pb$ and $^{24}Mg + ^{12}C$ systems, calculated using the ECIS94 coupled-channels code [18]. The contributions arising from Coulomb and nuclear excitations are presented. At 32 A MeV, most of the inelastic cross section is covered by our experimental angular range of zero to 10 degrees. Contrary to higher incident energies, for ^{208}Pb the contribution of the nuclear amplitude to the integrated inelastic cross section is significant only for angles larger than the Fresnel maximum. The contribution of higher lying excited states, which decay to the first 2^+ state — the feeding cross-section $\sigma_{\mathrm{feed}}(J^\pi \to 2^+)$ — has to be subtracted to obtain the experimental excitation cross-sections $\sigma_{\mathrm{exc}}(0^+ \to 2^+)$. In the case of

Table 1
The quantities $S_{\mathrm{exp}}(\mathrm{Si}_k)$ and $\sigma_{\mathrm{exp}}(\mathrm{Si}_k)$ are defined in the text. We also present the adopted values of the experimental angle integrated de-excitation cross-sections σ_{exp}, the calculated feeding cross-sections and the experimental angle-integrated excitation cross-sections σ_{exc}, for the six systems studied

System	$S_{\mathrm{exp}}(\mathrm{Si}_3)$ (mb)	$S_{\mathrm{exp}}(\mathrm{Si}_2)$ (mb)	$S_{\mathrm{exp}}(\mathrm{Si}_1)$ (mb)	$\sigma_{\mathrm{exp}}(\mathrm{Si}_3)$ (mb)	$\sigma_{\mathrm{exp}}(\mathrm{Si}_2)$ (mb)	$\sigma_{\mathrm{exp}}(\mathrm{Si}_1)$ (mb)	σ_{exp} (mb)	σ_{feed} (mb)	σ_{exc} (mb)
	0–2.1°	2.1–4.5°	4.5–10°				$2^+ \to 0^+$	$J^\pi \to 2^+$	$0^+ \to 2^+$
$^{24}\mathrm{Mg}+^{208}\mathrm{Pb}$	–	64 ± 10	268 ± 26	–	386 ± 63	432 ± 47	422 ± 46	89 ± 7	333 ± 46
$^{30}\mathrm{Mg}+^{208}\mathrm{Pb}$	–	109 ± 15	251 ± 22	–	367 ± 40	418 ± 45	402 ± 43	50 ± 10	352 ± 44
$^{32}\mathrm{Mg}+^{208}\mathrm{Pb}$	–	164 ± 30	276 ± 39	–	560 ± 72	544 ± 60	550 ± 72	44 ± 10	505 ± 73
$^{24}\mathrm{Mg}+^{12}\mathrm{C}$	53 ± 4	21 ± 3	–	67 ± 6	92 ± 9	–	76 ± 8	27 ± 6	49 ± 9
$^{30}\mathrm{Mg}+^{12}\mathrm{C}$	53 ± 5	8 ± 2	–	57 ± 6	64 ± 7	–	61 ± 7	15 ± 5	46 ± 8
$^{32}\mathrm{Mg}+^{12}\mathrm{C}$	65 ± 6	–	–	70 ± 9	–	–	70 ± 9	13 ± 4	57 ± 10

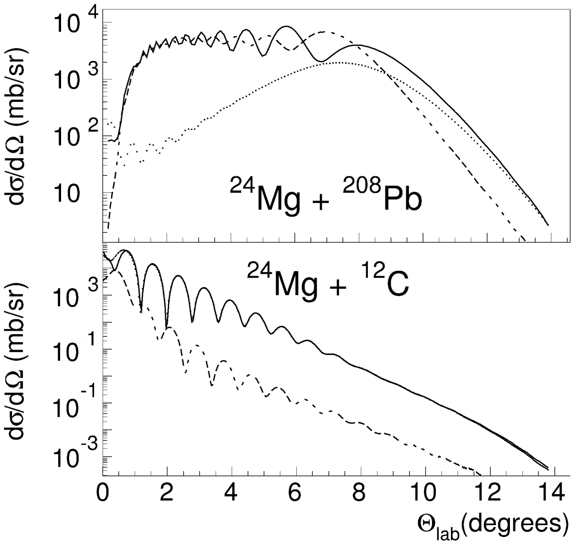

Fig. 3. Calculated inelastic angular distribution for the reactions $^{24}\mathrm{Mg}+^{208}\mathrm{Pb}$ and $^{24}\mathrm{Mg}+^{12}\mathrm{C}$. The contributions arising from nuclear and Coulomb excitations are represented by the dotted and dashed lines, respectively.

^{24}Mg the level scheme is known and the feeding cross section was calculated using the code ECIS94 with two coupling schemes and optical potentials: (i) an asymmetric rotational model with the $K = 0$ ground-state band and the $K = 2$ band (based on the 2_2^+ state) coupled together and direct excitation of the 3^- and 1^- states up to 11.4 MeV (a total of 13 excited states), (ii) a symmetric rotational model with direct excitation of the 2^+, 3^- and 1^- states up to 11.4 MeV. The same deformation lengths, βR were used for the charge and mass distributions ($\beta_2^c = \beta_2^N = 0.606$ with $R_N = R_c = 1.20\ A^{1/3}$) of the rotational bands. They were obtained assuming the adopted value of $B(\mathrm{E2}) = 432 \pm 12\ e^2\,\mathrm{fm}^4$ [11] for ^{24}Mg and the relation

$$B\big(\mathrm{E2}, 0^+ \to 2^+\big) = \big[(3/4\pi) Ze R_c^2 \beta_2^c\big]^2. \qquad (2)$$

In the first coupling scheme both the optical potential of Barrette et al. [19] (Pot.B) and the proximity potential [20] (Pot.P1 for $^{24}\mathrm{Mg}+^{208}\mathrm{Pb}$: $V = W = 65.80$ MeV, $r_r = r_i = 1.21$ fm and Pot.P2 for $^{24}\mathrm{Mg}+^{12}\mathrm{C}$: $V = W = 41.30$ MeV, $r_r = r_i = 1.141$ fm and diffusivity $a_r = a_i = 0.630$ fm for both) were used. The angular variation of S_{exp} was well reproduced by both potentials. After weighting the calculated excitation cross-sections for the higher lying excited states by the respective branching ratios for decay to the first 2_1^+, the total feeding to the first 2_1^+ state was deduced. It should be noted that the contribution from individual states depends to some extent on the coupling scheme used, however the sum of all contributions is quite similar and within the experimental uncertainties in the measured cross-sections. The cross-sections are presented in Table 2, where the direct excitation of the first 2^+ state in presence of couplings, the feeding of the first 2^+ state by higher lying states, and the sum (the total calculated de-excitation cross-section) are listed. The cross-sections have similar values for the two optical potentials used, even in

Table 2
The calculated cross-sections for direct excitation of the first 2^+ state in ^{24}Mg in the presence of couplings, for the feeding of the first 2^+ state by higher-lying states and their sum, the total calculated de-excitation cross-section, to be compared with the total experimental de-excitation cross-section (last column). Potentials B, P1 and P2 are defined in the text

System	Pot.	$\sigma(0^+ \to 2^+)$ (mb)	σ(feeding) (mb)	$\sigma(2^+ \to 0^+)$ (mb)	$\sigma_{\text{exp}}(2^+ \to 0^+)$ (mb)
$^{24}\text{Mg} + {}^{208}\text{Pb}$	B	367	85	452	422 ± 46
	P1	378	95	473	
$^{24}\text{Mg} + {}^{12}\text{C}$	B	54	24	78	76 ± 8
	P2	52	27	79	

the case of the ^{12}C where the nuclear interaction is dominant. Very good agreement is observed between the experimental and calculated de-excitation cross-sections (Table 2) for the first 2^+ state of ^{24}Mg, for reactions on both ^{208}Pb and ^{12}C, demonstrating the reliability of the method.

The level schemes of ^{30,32}Mg nuclei are not so well known as of ^{24}Mg, and we cannot make a detailed calculation of the feeding contributions as we did for ^{24}Mg. The feeding contributions for ^{30,32}Mg were consequently estimated by scaling the feeding cross-section of ^{24}Mg according to the one-proton separation energy S_p (11.63 MeV) in ^{24}Mg and the one-neutron separation energy S_n, 6.29 MeV in ^{30}Mg and 5.65 MeV in ^{32}Mg. This correction is based on the assumption that the total feeding cross-section should be proportional to the highest excitation energy which still decays by γ-emission, i.e., to the one proton separation energy for ^{24}Mg and the one neutron separation energy for ^{30,32}Mg. The detailed calculations of the feeding contribution included not only the decay from the next excited state (most probably 4^+), as in the analysis of Ref. [13], but also all possible contributions from higher lying states. Table 1 includes the total de-excitation cross-sections, the calculated feeding cross-sections, and the difference corresponding to the estimated experimental excitation cross-section of the first 2^+ state, $\sigma_{\text{exc}}(0^+ \to 2^+)$.

The excitation cross-section calculated with the ECIS94 code with a symmetric rotational form factor with two deformation lengths, the charge and optical deformation lengths $\beta_c R_c$ and $\beta_{\text{opt}} R_{\text{opt}}$ as free parameters, in order to reproduce the experimental excitation cross-sections $\sigma_{\text{exc}}(0^+ \to 2^+)$ on both targets. The mass deformation length was obtained under the assumption of $\beta_N R_N = \beta_{\text{opt}} R_{\text{opt}}$. The inelastic excitation induced by ^{208}Pb depends mainly on $\beta_c R_c$ and little on $\beta_N R_N$ over the angular range considered here. In contrast, in the case of ^{12}C induced excitation, the main contribution comes from $\beta_N R_N$. When describing the scattering of one Mg isotope on both targets, we use the same Coulomb and nuclear deformation lengths $\beta_c R_c$ and $\beta_N R_N$ (with $R_c = R_N = 1.20\ A^{1/3}$ fm). The calculations were performed with the different optical potentials quoted above (B, P1, P2) and the final uncertainty in the β-values includes the effect of the uncertainty in the optical potentials.

The deformation parameters β_c and β_N obtained in this way for ^{30}Mg and ^{32}Mg are presented in Table 3, together with the results of calculations. An important feature can be observed immediately: the charge and mass deformations are identical within the uncertainties for both nuclei. This result is in agreement with the predictions of Refs. [7,8,10] and in variance with the predictions of Refs. [6,9]. The $B(\text{E2})$ values were calculated from the β_c values using $R_c = 1.20\ A^{1/3}$ fm and Eq. (2) and they are presented in Table 4 together with previous experimental and theoretical results. Our $B(\text{E2})$ value for ^{32}Mg agrees within uncertainties with the results of [12], while our $B(\text{E2})$ values for ^{30,32}Mg are significantly higher than the values reported in Ref. [13]. For ^{32}Mg, the results of the standard shell model [4,6] calculations are in reasonable agreement with our measured values. The HFB calculations of Ref. [21] predict lower transition probabilities for ^{30,32}Mg. The constrained HF calculations of Ref. [10] with a separable interaction pre-

Table 3
The deformation parameters and deformation lengths of ^{24,30,32}Mg compared with calculations

	This work				Ref. [7]		Ref. [6]		Ref. [10]	
	β_c	β_N	$\beta_c R_c$	$\beta_N R_N$	$\beta_c R_c$	$\beta_N R_N$	$\beta_c R_c$	$\beta_N R_N$	$\beta_c R_c$	$\beta_N R_N$
^{24}Mg	0.57 ± 0.04	0.57 ± 0.052	1.97 ± 0.14	1.97 ± 0.18	1.45	1.37	–	–	2.50	2.35
^{30}Mg	0.52 ± 0.035	0.50 ± 0.045	1.95 ± 0.13	1.86 ± 0.17	0.91	0.73	–	–	1.97	1.82
^{32}Mg	0.61 ± 0.044	0.54 ± 0.05	2.31 ± 0.17	2.08 ± 0.19	1.34	1.41	1.45	0.91	1.96	1.84

Table 4
The reduced transition probabilities $B(\mathrm{E2}, 0^+ \to 2^+)$ of ^{24,30,32}Mg. The adopted value of $B(\mathrm{E2}, 0^+ \to 2^+)$ of ^{24}Mg is 432 e^2 fm^4. The results of this work are compared with previous experimental results and calculations. The B(E2) values of Ref. [6] were obtained from 2p–2h and 4p–4h ground-state configurations for ^{32}Mg and 0p–0h for ^{30}Mg

	This work	Ref. [12]	Ref. [13]	Ref. [6]	Ref. [21]	Ref. [10]	Ref. [22]
	B(E2) e^2 fm^4	B(E2) e^2 fm^4	B(E2) e^2 fm^4	B(E2) e^2 fm^4	B(E2) e^2 fm^4	B(E2) e^2 fm^4	B(E2) e^2 fm^4
^{24}Mg	383 ± 53	–	–	–	–	616	–
^{30}Mg	435 ± 58	–	295 ± 26	242	200	442	182
^{32}Mg	622 ± 90	454 ± 78	333 ± 70	490/650	333	456	593

dict similar and large deformations for both ^{30,32}Mg. In Ref. [22] a microscopic angular momentum projection after variation is used to describe quadrupole collectivity in ^{30,32,34}Mg. The Hartree–Fock–Bogoliubov states obtained in the quadrupole constrained mean-field approach are taken as intrinsic states for the projection. For ^{32}Mg the B(E2) value agrees very well with our experimental value, while for ^{30}Mg the predicted value is much lower than our experimental result.

In conclusion, we have extracted the Coulomb and nuclear deformation lengths of ^{30,32}Mg by the inelastic excitation measurements of intermediate energy secondary beams on ^{208}Pb and ^{12}C targets. Both nuclei exhibit similarly large charge and mass deformations. The analysis within the collective model resulted in identical mass and charge deformations, giving no evidence for a large decoupling of neutron and proton deformations in this region. The ^{30}Mg nucleus exhibits a much larger transition strength than previously predicted, raising the question of a strong collective behaviour and its belonging to the “island of inversion”.

Acknowledgements

V.C. wishes to thank CNPq and CEA for financial support received.

References

[1] N.A. Orr et al., Phys. Lett. B 258 (1991) 29, and references therein.
[2] A. Poves, J. Retamosa, Phys. Lett. B 184 (1987) 311.
[3] E.K. Warburton, J.A. Becker, B.A. Brown, Phys. Rev. C 41 (1990) 1147.
[4] N. Fukunishi, T. Otsuka, T. Sebe, Phys. Lett. B 296 (1992) 279.
[5] A. Poves, J. Retamosa, Nucl. Phys. A 571 (1994) 221.
[6] E. Caurier et al., Phys. Rev. C 58 (1998) 2033.
[7] D. Hirata, private communication.
[8] Y. Kanada-Enyó, private communication.
[9] J. Terasaki et al., Nucl. Phys. A 621 (1997) 706.
[10] P.D. Stevenson, J. Rikovska Stone, M.R. Straayer, to be published.
[11] S. Raman et al., At. Data Nucl. Data Tab. 36 (1987) 1–96.
[12] T. Motobayashi et al., Phys. Lett. B 346 (1995) 9.
[13] B.V. Pritychenko et al., Phys. Lett. B 461 (1999) 322.
[14] R. Anne, A.C. Mueller, Nucl. Instrum. Methods B 70 (1992) 276.
[15] D. Guillemaud-Mueller et al., Nucl. Phys. A 426 (1984) 37.

[16] G. Klotz et al., Phys. Rev. C 47 (1993) 2502.
[17] P.M. Endt, Nucl. Phys. A 521 (1990) 1.
[18] J. Raynal, Coupled-Channels code ECIS94 unpublished.
[19] J. Barrette et al., Phys. Lett. B 209 (1988) 182.
[20] R.A. Broglia, A. Winther, Heavy Ion Reactions, Vol. 1, Benjamin/Cummings, 1981.
[21] M. Girod, private communication.
[22] R. Rodriguez-Guzman, J.L. Egido, L.M. Robledo, Phys. Lett. B 474 (2000) 15.